⌘ *Author's Choice*

THE JOURNAL OF BIOLOGICAL CHEMISTRY VOL. 285, NO. 52, pp. 41135–41142, December 24, 2010

Resting State Orai1 Diffuses as Homotetramer in the Plasma Membrane of Live Mammalian Cells*[S]

Received for publication, August 23, 2010, and in revised form, October 5, 2010 Published, JBC Papers in Press, October 20, 2010, DOI 10.1074/jbc.M110.177881

Josef Madl, Julian Weghuber, Reinhard Fritsch, Isabella Derler, Marc Fahrner, Irene Frischauf, Barbara Lackner[1], Christoph Romanin, and Gerhard J. Schütz[2]

From the Biophysics Institute, Johannes Kepler University Linz, Altenbergerstrasse 69, A-4040 Linz, Austria

Store-operated calcium entry is essential for many signaling processes in nonexcitable cells. The best studied store-operated calcium current is the calcium release-activated calcium (CRAC) current in T-cells and mast cells, with Orai1 representing the essential pore forming subunit. Although it is known that functional CRAC channels in store-depleted cells are composed of four Orai1 subunits, the stoichiometric composition in quiescent cells is still discussed controversially: both a tetrameric and a dimeric stoichiometry of resting state Orai1 have been reported. We obtained here robust and similar FRET values on labeled tandem repeat constructs of Orai1 before and after store depletion, suggesting an unchanged tetrameric stoichiometry. Moreover, we directly visualized the stoichiometry of mobile Orai1 channels in live cells using a new single molecule recording modality that combines single molecule tracking and brightness analysis. By alternating imaging and photobleaching pulses, we recorded trajectories of single, fluorescently labeled Orai1 channels, with each trajectory consisting of bright and dim segments, corresponding to higher and lower numbers of colocalized active GFP label. The according brightness values were used for global fitting and statistical analysis, yielding a tetrameric subunit composition of mobile Orai1 channels in resting cells.

Store-operated calcium entry is a mechanism where the decrease of the calcium concentration in the endoplasmic reticulum (ER)[3] triggers the influx of extracellular calcium into the cytoplasm (1). Entry of extracellular calcium is essential, *e.g.* for prolonged calcium signaling or for refilling the calcium stores. The best studied store-operated calcium current is the calcium release-activated calcium (CRAC) current in T-cells and mast cells, I_{crac} (2). The key players in I_{crac} are STIM1 and Orai1. STIM1 is an ER membrane protein that senses the ER calcium concentration via a luminal EF-hand (3, 4). Store depletion leads to oligomerization and subsequent clustering of STIM1 in close proximity to the plasma membrane (5, 6). STIM1 directly interacts with Orai1, a plasma membrane-located protein (7, 8), which co-clusters with STIM1 in micrometer sized ER-plasma membrane junctions upon store depletion. Orai1 was identified as the essential pore-forming subunit of the CRAC channel (9–11).

As Orai1 has only four transmembrane domains and shows no known homology to other calcium channels, there soon have been speculations regarding the subunit stoichiometry of the channel. First, biochemical assays revealed the existence of Orai1 dimers; tetramers were found after the addition of a chemical cross-linking agent (12). By introducing cysteines at specific sites in Orai1 subunits and applying disulfide cross-linking assays, it was concluded that Orai1 assembles as a tetramer or as a higher oligomer (13). A study employing electron microscopy reported a tetrameric stoichiometry of purified Orai1 proteins (14). Coexpression of preassembled tandem Orai1 multimers with a dominant-negative mutant revealed that functional pores are formed by tetrameric Orai1 assemblies (15). More detailed insights were obtained by direct single molecule imaging approaches (16, 17); following the steps in single molecule photobleaching curves allowed for counting the number of colocalized GFP-tagged subunits (18, 19). Whereas Ji *et al.* (16) observed exclusively Orai1 tetramers in fixed HEK-293 cells, Penna *et al.* (17) reported Orai dimers in resting *Xenopus laevis* oocytes that associated to tetramers only upon coexpression of the STIM C terminus. The latter data were particularly interesting as they suggested a unique mechanism for the activator protein STIM to assemble the functional Orai tetramer.

Due to the apparent discrepancy between the results of the two single molecule studies and their restriction to the analysis of immobile or immobilized proteins, we decided to design a more versatile approach, which allows for the determination of the subunit stoichiometry of mobile resting state Orai1. Our rationale was that mobile subfractions provide the cleanest pool of data, devoid of contributions, *e.g.* from potentially preassociated STIM1-Orai1 complexes or vesicles attached to the plasma membrane; moreover, resting state Orai1 is predominantly mobile (8), and mobility appears critical for the lateral redistribution upon store depletion. In this report, we describe the methodology and provide evidence that in mam-

* This work was supported by the Austrian Science Fund (Ph.D. Program W1201 "Molecular Bioanalytics" and project Y250-B3 to G. J. S.; Project P2118 to C. R.: and Hertha Firnberg T466-B09 to I. D.) and the GEN-AU project of the Austrian Research Promotion Agency.

⌘ *Author's Choice*—Final version full access.

[S] The on-line version of this article (available at http://www.jbc.org) contains supplemental Figs. S1–S6 and Movies S1–S3.

[1] Recipient of a DOC-forte scholarship of the Austrian Academy of Sciences.

[2] To whom correspondence should be addressed: Biophysics Institute, Johannes-Kepler-University Linz, Altenbergerstr. 69, A-4040 Linz, Austria. Tel.: 43-732-2468-9284; Fax: 43-732-2468-29284; E-mail: gerhard.schuetz@jku.at.

[3] The abbreviations used are: ER, endoplasmic reticulum; mGFP, monomeric green fluorescent protein; CRAC, calcium release activated calcium current; BHQ, 2,5-di-t-butyl-1,4-benzohydroquinone; FRAP, fluorescence recovery after photobleaching; TOCCSL, thinning out clusters while conserving the stoichiometry of labeling; CFP, cyan fluorescent protein; YFP, yellow fluorescent protein.

malian cells mobile resting state Orai1 shows tetrameric assembly.

EXPERIMENTAL PROCEDURES

Orai1 Constructs—Orai1 tandem repeat constructs were subcloned from pcDNA3.1/V5-His TOPO vector (Invitrogen) via internal restriction sites BglII/SalI and BamHI/XbaI and cloned into ECFP and EYFP-C1 (Clontech). To generate the Orai1-mGFP-N1 construct, monomeric GFP (20) was amplified from pJB20-GPI-mGFP (21) using the forward primer 5′-ATATATACCGGTAATGAGCAAGGGCGAGGAGC-TGTTC-3′ and the reverse primer 5′-CTCGGCATGGAC-GAGCTGTACAAGTAAGCGGCCGCATATAT-3′. The PCR product was digested with AgeI and NotI and cloned into the Orai1-YFP-N1 vector (7) digested with the same restriction enzymes. All resulting constructs were confirmed by sequencing.

Cell Lines—HEK-293 cells were cultured at 37 °C and 8.5% CO_2 in DMEM (PAA Laboratories) supplemented with 10% FBS (Invitrogen) and penicillin/streptomycin (PAA). For FRET and electrophysiology experiments, cells were transferred to glass coverslips in 35-mm dishes 2 days before the experiments and transfected using TransFectin (Bio-Rad) according to the manufacturer's instructions on the day before the experiment. T24 cells were cultured in RPMI 1640 medium supplemented with 10% FBS, penicillin/streptomycin (PAA), and grown at 37 °C in a humidified incubator with 5% CO_2. 70% confluent cells were harvested and transfected with 10 μg Orai1-mGFP-N1 plasmid DNA using the X-Cell electroporator (Bio-Rad) with following electroporation settings: 240 V, 950 μF, unlimited resistance, 4-mm gap cuvettes. Cells were plated into 100-mm culture dishes and grown for 48 h. The medium was removed and replaced with fresh medium supplemented with 400 μg/ml G418. Medium was changed every 3 days, and 15–20 days later, individual neomycin-resistant colonies were selected for further propagation. T24-Orai1-mGFP cells were passaged 1–2 days before experiments and seeded on glass slides, which have been coated with 10 μg/ml fibronectin (Sigma-Aldrich) for 45 min at room temperature. For characterization of STIM1/Orai1 coupling, T24-cells were transfected using TransFectin according to the manufacturer's instructions 2 days before the experiments and seeded on glass slides 1 day before the experiment.

FRET Measurements—FRET measurements were performed on an inverted microscope (Axiovert 200 M, Zeiss) equipped with a Nipkow disk confocal scanner according to Muik *et al.* (7). The light source was a multiline Ar^+-laser combined with an acousto-optic tunable filter. The illumination time was 900 ms. Fluorescence emission was separated using a long pass filter (505 LP) and two emission filters for CFP and YFP and recorded on two cameras (CoolSNAP HQ, Photometrics). The setup was controlled using MetaMorph 5 (Universal Imaging). Cells were transfected with CFP-Orai1-Orai1 and YFP-Orai1-Orai1 and optionally STIM1. For the measurements, the coverslips were mounted in a cell bath containing an extracellular buffer solution with 2 mM calcium. Stores were depleted using 2 μM thapsigargin (Sigma-Aldrich). All FRET experiments were performed at room temperature. FRET was evaluated using the normalized FRET method of Xia and Liu (22). Briefly, FRET images were corrected for cross-talk and direct excitation. Calibration values were obtained from cells expressing only the CFP- or YFP-labeled constructs. Images were analyzed on a pixel per pixel basis using custom-made programs in Matlab as described in more detail in Ref. 7.

Electrophysiology—HEK-293 cells were transfected with CFP-STIM1 and either YFP-Orai1 or YFP-Orai1-Orai1-tandem repeat constructs. Measurements were carried out in paired comparison on the same day. Expression pattern and levels of the Orai1 constructs in HEK cells were examined carefully by confocal fluorescence microscopy and were not significantly different due to the linkage of two Orai1 proteins. For testing Orai1-mGFP functionality, HEK-293 cells were transfected with Orai1-mGFP and mCherry-STIM1. For store depletion, the internal pipette solution contained the following: 145 mM caesium methane sulfonate, 8 mM NaCl, 3.5 mM $MgCl_2$, 10 mM HEPES, 10 mM EGTA, and pH was 7.2. To prevent store depletion, the internal pipette solution contained 100 nM free Ca^{2+} by additionally including 4.3 mM Ca^{2+}. Extracellular solution consisted of the following: 145 mM NaCl, 5 mM CsCl, 1 mM $MgCl_2$, 10 mM HEPES, 10 mM glucose, 10 mM $CaCl_2$, pH 7.4. Wild-type T24 cells and T24 cells stably expressing Orai1-mGFP were compared using a whole-cell recording configuration under resting state conditions. The internal pipette solution included the following: 3.5 mM $MgCl_2$, 145 mM caesium methane sulfonate, 8 mM NaCl, 10 mM HEPES, 10 mM EGTA, 4.3 mM $CaCl_2$. For blocking of Orai1 channels, 10 μM lanthan was added after 300 s of recording. For current measurements, voltage ramps were usually applied every 5 s from a holding potential of 0 mV, covering a range of −90 to 90 mV for 1 s. All electrophysiological experiments were performed at room temperature.

STIM1/Orai1 Coupling in T24 Cells—Characterization experiments (see Fig. 2*A*) were performed on a home-built epifluorescence scanning microscope (23) based on a commercial Axiovert 200 body (Zeiss). The samples were illuminated in total internal reflection configuration with the 488-nm line of an Ar^+-laser (Innova, Coherent) via a 100× objective (numerical aperture, 1.45, α-Fluar, Zeiss). Fluorescence was imaged onto a back-illuminated CCD camera (NTE/CCD-1340/100-EMB, Roper Scientific). Single band filters for CFP, YFP, and GFP were used for the respective fluorophores (Chroma). T24 cells were transfected using YFP-Orai1 and CFP-STIM1. Expression of both constructs was checked prior to store-operated calcium entry activation. Stores were depleted using 30 μM 2,5-di-*tert*-butylhydroquinone (BHQ, Sigma-Aldrich) in Hanks' buffered saline solution without calcium and magnesium. During store depletion, the YFP channel was monitored. The same store depletion protocol was used for T24 cells stably expressing Orai1-mGFP. These experiments were performed at room temperature.

Brightness and Mobility Experiments—Single molecule fluorescence and fluorescence recovery after photobleaching (FRAP) experiments were performed on a customized epifluorescence microscope (Axiovert 200, Zeiss). Samples were illuminated via a 100× objective (Plan-Apochromat; numerical aperture, 1.45;

Zeiss) using the 488-nm line of an Ar^+-ion laser (Stabilite 2017-AR, Spectra Physics) either in total internal reflection or conventional epifluorescence configuration. An acousto-optical modulator (model 1205C, Isomet) was used to control both illumination time and excitation power. The acousto-optical modulator was operated as outlined below (see Fig. 3*A*) for single molecule measurements. For FRAP analysis, an $\sim 3.5 \times 3.3\ \mu m^2$ region was bleached at high power for 600 ms. For brightness analysis, a region of $\sim 17 \times 17\ \mu m^2$ was bleached. We used two power levels, 5.2 kilowatts/cm^2 at the object plane (*high* in Fig. 3*A*) and 180 watts/cm^2 (*low* in Fig. 3*A*). The illumination time for imaging was set to 50 ms at low power. A fast-spinning diffuser disk was placed in the beam path to homogenize the illumination profile at the sample. Excitation light and fluorescence emission were separated using a GFP dichroic and emission filter (Semrock). Fluorescence signals were recorded on a back-illuminated liquid nitrogen-cooled CCD camera (Micro Max 1300-PB, Roper Scientific). The camera chip was operated in kinetics mode to achieve minimal delay times between consecutive images of $t_{del} = 1$ ms. Due to the kinetics mode the number of readout images per measuring sequence was limited. The region of interest in *y* direction was reduced to 50 pixels in the central part of the photobleached area, which allowed for acquiring of 23 images per sequence. The microscope was equipped with a temperature control system (POCmini, Zeiss) and a home-built temperature box. All single molecule fluorescence and FRAP experiments were performed at 37 °C.

FRAP Analysis—Data were analyzed using our algorithms implemented in Matlab (MathWorks). For FRAP analysis of the mobile fraction, the central part of the bleached region was evaluated by integrating all counts and normalizing to the prebleach image. The FRAP curve in the inset shown in Fig. 2*C* shows mean and S.D. from measurements on 11 T24-Orai1-mGFP cells.

Data Analysis—For diffusion analysis, the positions of single Orai1 pores $\vec{r}$ were determined with Matlab software as described previously (24). Mean square displacements were calculated for various time lags (t_{lag}). The diffusion coefficient was determined from the slope of a linear regression of the first two data points in the plot according to Equation 1.

$$MSD(t_{lag}) = \langle \vec{r}(t_{lag})^2 \rangle = 4 \cdot D \cdot t_{lag} + c_{offset} \qquad \text{(Eq. 1)}$$

The negative offset of the linear regression is a consequence of the molecular motion during the illumination (24, 25).

For brightness analysis, a 3×3 pixel square (*i.e.* 600×600 nm) was centered at the brightest pixel of a diffraction limited fluorescent spot (see Fig. 3*D*). The background was estimated from a 5×5 pixel ring surrounding this area. Continuous probability density functions were generated from the discrete data sets using a kernel smoothed density estimate (ksdensity, Matlab).

The brightness of different numbers of colocalized copies of mGFP was approximated using Gaussian functions (26–28). Accordingly, a set of three linear combinations of *n* Gaussians was used to model the entire brightness distribution (where $j = 1$, 2, or 3),

$$p_j(B)dB = \sum_{i=1}^{N} \frac{\alpha_{ij}}{\sigma_i \sqrt{2\pi}} \cdot exp^{-\frac{1}{2}\left(\frac{B-\mu_i}{\sigma_i}\right)^2} dB \qquad \text{(Eq. 2)}$$

where $p_j(B)$ denotes the probability for measuring the brightness (B) for data set j. N is the total number of Gaussians used for the respective function set to model the brightness distributions, *i.e.* the presumed number of mGFPs per Orai1 pore. Index (i) is used for indexing the individual Gaussians. For the global fit, the same means μ_i and widths σ_i were used to fit the three data sets, whereas the weights α_{ij} were allowed to vary throughout the distinct data sets. The sum of the weights α_{ij} was constrained to be 1 for each data set j. The three data sets were fitted globally using a least-square nonlinear fitting routine, yielding the fit parameters (μ_i, σ_i, α_{ij}; $i = 1, \ldots, N$; $j = 1, 2, 3$) according to the model used. The starting parameters were chosen from visual inspection of the individual brightness distributions. The stability of global fitting was tested by randomly varying all starting parameters in a reasonable range. The fits using 2- and 4-Gaussians were extremely stable, the results of the 3- and 5-Gaussian fits slightly varied depending on the starting parameters. The goodness of the fits was compared using the overall norm of the residuals (see Table 1).

We used a nonparametric statistical test to estimate *p* values for the tetramer and dimer model (29). For this, we took the fit parameters determined for the three data sets as basis for a Monte Carlo simulation of the brightness distributions, assuming either a dimer or a tetramer model. The simulation results were compared with the original data by a two-sample Kolmogorov-Smirnov hypothesis test. This algorithm was repeated 50 times.

RESULTS

Store Depletion Does Not Affect Association State of Covalently Linked Orai1 Homodimers—In an attempt to approach the dimer-to-tetramer transition of Orai1, which might occur in response to store depletion, we initially generated a covalently linked Orai1 homodimer and followed a potential alteration of FRET between CFP/YFP-labeled dimers upon stimulation of their coupling to STIM1 by thapsigargin. These tagged Orai1-homodimers, when co-expressed in HEK-293 cells together with STIM1, were functionally active as evaluated in electrophysiological experiments; experiments on the Orai1 homodimers or on their monomeric form led to the same store-operated current activation (Fig. 1, *A* and *B*). FRET as an indicator for association between Orai1 homodimers amounted already to robust values of 0.26 ± 0.04 ($n = 6$) at the resting state of the cell, which did not significantly change upon store depletion by thapsigargin (Fig. 1, *C* and *D*). Similar FRET values were also observed in the absence of coexpressed STIM1 (0.24 ± 0.03, $n = 7$, Fig. 1*D*, supplemental Fig. S1). Based on these experiments, a tetrameric state of Orai1 independent of the association with STIM1 seemed more likely than a dimeric resting state assembly.

Characterization of a Stable Orai1-mGFP-expressing Cell Line—To assess the stoichiometry more directly, we established single molecule microscopy on mobile Orai1 proteins

expressed in living mammalian cells. For this, subunits were labeled by fusing them to a monomeric variant of the GFP (Orai1-mGFP, (20)). Because each Orai1 subunit is labeled with exactly one fluorophore, the brightness of a single Orai1-mGFP channel can be used as a direct measure of the number of subunits present in this assembly. For stoichiometry measurements, we used a human bladder carcinoma cell line (T24) as an expression system, which allowed for single molecule resolution with a much better signal to noise ratio than that observed in HEK-293 cells. We used overexpression of mGFP-labeled Orai1 to avoid a potential association with significant amounts of endogenous subunits, which would result in an underestimation of the stoichiometry. The store-dependent function of Orai1-mGFP was confirmed in HEK-293 cells coexpressing STIM1 (supplemental Fig. 2). Fig. 2 shows experiments for the characterization of the Orai1 functionality in T24 cells. A possible influence of endogenous STIM1 was assessed by depleting the Ca^{2+} stores in the ER using BHQ. Store depletion of T24 cells expressing both STIM1 and Orai1 induced strong clustering of the latter within minutes (Fig. 2*A*), whereas no clustering was observed in cells overexpressing Orai1 alone. We conclude that the massive redistribution of Orai1 preceding store-operated calcium can be induced in the chosen cell system. Electrophysiological experiments in the stable T24-Orai1-mGFP cell line indicated only minor leak current densities under conditions to prevent ER store depletion (100 nM intracellular Ca^{2+}, reversal potential ~0 mV), which were not significantly different to those of control T24 cells over a time period of 300 s (Fig. 2*B*). Moreover, the typical Orai1 channel blocker La^{3+} did not alter basal leak current levels in both cell lines confirming the absence of Orai1 current activation. Thus, based on the lack of Orai1 clustering and current activation, we were fairly safe that under the conditions used for the subsequent stoichiometry experiments, the cells were in a resting state and the Orai1-mGFP channels in a silent state uncoupled from STIM1.

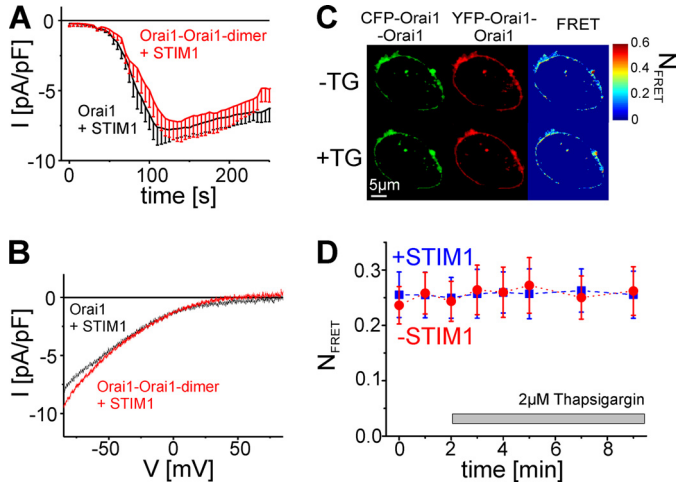

FIGURE 1. **Orai1-Orai1 tandem repeat constructs in HEK-293 cells.** *A* and *B*, whole-cell patch clamp experiments on HEK-293 cells expressing STIM1 and either the monomeric Orai1 subunit (*black*) or the Orai1-Orai1 tandem construct (*red*). Stores were depleted passively by using 10 mM EGTA in the pipette solution, yielding comparable currents for both constructs. *A*, time course of mean currents recorded at −74 mV during voltage ramps ($n = 6$ for Orai1-Orai1 dimer, $n = 9$ for Orai1). *B*, *I-V* curve recorded 150 s after break in. *C*, HEK-293 cells expressing STIM1 and the two tandem repeat constructs CFP-Orai1-Orai1 and YFP-Orai1-Orai1 showed comparable FRET before and after store depletion via 2 µM thapsigargin (*upper* and *lower panels*, respectively). *D*, time course of FRET for HEK-293 cells expressing CFP-and YFP-labeled Orai1-Orai1 constructs with (*blue*) and without (*red*) coexpression of STIM1. Thapsigargin was added after 2 min. All *error bars* denote standard errors of the mean.

Resting State Orai1 Diffuses Freely in Plasma Membrane—We next attempted to address individual Orai1 channels, as they move in the plasma membrane of living T24 cells. In general, however, the high expression level precluded direct imaging of single channels as diffraction-limited spots (see Fig. 2*A* and Fig. 3*C*); we estimated a surface density of ~100–500 channels per μm^2. When we totally photobleached a rectangular area (size ~ 3.5 × 3.3 μm^2), the fluorescence signal recovered on a time scale of minutes, yielding a mobile fraction of 91 ± 9% (Fig. 2*C*, *inset*), which is in agreement with previously published literature (8).

Tracking of single molecules in living cells is preferentially performed under total internal reflection excitation, so that cytosolic fluorescent background can be substantially reduced (30). In such a configuration, membrane-anchored fluorescent tracers would recover from the edges of the bleached region, whereas recovery from potential cytosolic populations would emerge uniformly over the whole area. However, at the onset of the recovery process, we frequently observed the sudden appearance of fluorescent spots all over the photobleached region, when we used total internal reflection excita-

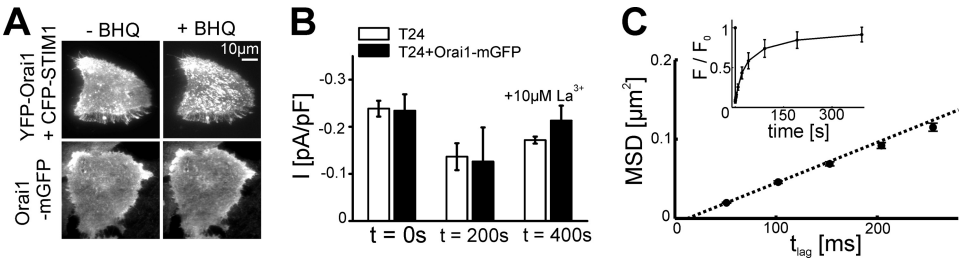

FIGURE 2. **Characterization of the Orai1 functional state and mobility in T24 cells.** *A*, passive store depletion via BHQ in cells expressing both CFP-STIM1 and YFP-Orai1 led to the formation of Orai1 puncta in the plasma membrane (*top row*). In our standard T24 cell system stably transfected only with Orai1-mGFP, we did not observe this effect (*bottom row*). Images were recorded directly before and 9 min after addition of 30 µM BHQ. *B*, whole-cell patch clamp experiments of wild-type T24 cells (*white*) and T24 cells stable expressing Orai1-mGFP (*gray*) yielded similar results. Extracellular and intracellular solution contained 10 and 100 nM Ca^{2+}, respectively. *Bars* show mean values and S.E. ($n = 4$ for both cell lines). Currents measured directly after break in ($t = 0$ s), and also 100 s before ($t = 200$ s) and after ($t = 400$ s) the addition of 10 µM La^{3+}. *C*, mobility analysis of Orai1-mGFP in T24 cells. The mean square displacement increases linearly with time lag, indicating free diffusion with a diffusion coefficient of $D = 0.13$ μm^2/s. FRAP experiments (*inset*) revealed a mobile fraction of Orai1-mGFP of 91 ± 9% ($n = 11$ cells).

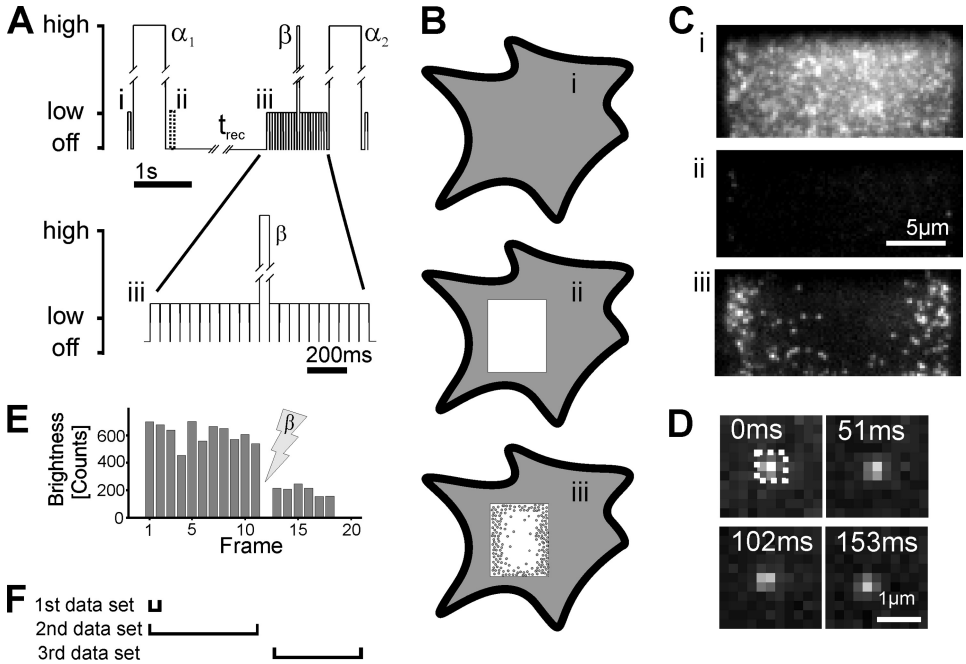

FIGURE 3. **Experimental strategy.** *A*, excitation protocol used for stoichiometry measurements. Imaging is performed at low excitation power (pulses *i*, *ii*, *iii* . . .). High power laser pulses are used for photobleaching of Orai1-mGFP. Pulses α_1 and α_2 completely destroy all active fluorophores within the photobleached area. The pulse β is shorter and results in only partial bleaching. Recording of images for the brightness analysis starts with readout pulse *iii*. *B*, scheme of the TOCCSL method. Overexpression of Orai1-mGFP results in a high density of labeled ion channels (*i*). Bleach pulse α_1 destroys all active fluorophores in a sharply defined area in a short time (*ii*). During the recovery time, nonbleached Orai1-mGFP pores enter the region of interest by diffusion (*iii*). In the center of the photobleached area molecules can be resolved and tracked. *C*, raw data were recorded as described in *B*. Intensity was downscaled by a factor of 3 for image *i*. *D*, the single channel brightness was determined on each image by integrating the photon counts in a 3 × 3 pixel region (*dotted line*). The background level was estimated from the surrounding 5 × 5 pixel ring. *E*, exemplary brightness trajectory of a single Orai1-mGFP spot. The brightness fluctuated at high levels (frames 1–11). The bleach pulse β reduced the fluorescence signal significantly. *F*, the illumination protocol allowed for grouping the recorded brightness values in three different data sets (see text for details).

tion (supplemental Movie S1). In contrast, the same experiment performed under conventional epi-illumination yielded no detectable single molecule signals at the same recovery time of 100ms (supplemental Movie S2). We conclude that, consistent with previous literature (31), also in T24 cells, a substantial fraction of Orai1-mGFP is located in cytosolic vesicles, which enter the depleted region of interest from the top, *i.e.* from the cytoplasm; when using standard epi-illumination, vesicles above the field of view are photobleached and thus do not contribute to the obtained postbleached images. In the following, we therefore performed all experiments under conventional epifluorescence excitation.

After longer recovery times of 30–90 s, membrane-anchored molecules start to fill the photobleached region by lateral diffusion from the edges (supplemental Movie 3). At these settings, individual Orai1 spots were well resolvable and trackable in the image center. By using mean-square displacement analysis, we observed free Brownian motion, characterized by a diffusion constant of $D = 0.13\ \mu m^2/s$ (37 °C, Fig. 2*C*, timing as shown in Fig. 3*A*); similar data were previously reported for eGFP-Orai1 (8). The free mobility further confirms that the studied Orai1-mGFP constructs do not interact with ER-localized endogenous STIM1.

Determination of Subunit Stoichiometry by Single Molecule Brightness Analysis—The brightness of the observed fluorescent spots contains information on the subunit stoichiometry of the corresponding ion channels. Indeed, single molecule tracking after photobleaching allows for thinning out clusters while conserving the stoichiometry of labeling (TOCCSL), as recently introduced for studying the association state of mobile membrane constituents (32, 33). The idea is sketched in Fig. 3*B*. A small part of a cell is totally photobleached by imaging a field stop onto the object plane (bleach pulse α_1 in the timing protocol shown in Fig. 3*A*); the achieved sharp (*i.e.* diffraction-limited) edges ensure that the brightness of fluorescent Orai1 pores located outside of the photobleached area remains unaffected by the bleaching protocol. Optional prebleach and postbleach images allow for determining the surface density and the efficiency of the bleaching pulse, respectively (images *i* and *ii* in Fig. 3*C*). All bleach pulses (α_1, α_2, and β) were applied at ~30-fold higher laser intensity than imaging pulses.

After the recovery time t_{rec}, a sequence of $n = 22$ consecutive images was recorded with an illumination time $t_{ill} = 50$ ms and a delay of $t_{del} = 1$ ms. The first image of this sequence (Fig. 3*C*, image *iii*) shows Orai1 channels well resolved and at their full brightness *B*. The recording of image number 12 was coupled to a second bleaching pulse (β), which was used for substantially reducing the brightness of the observed spots; the 10 remaining images contain Orai1 pores with lower number of active GFP molecules. Finally, a bleach pulse α_2 was used to erase the remaining GFPs in the region of interest, so that continuation of experiments on the same cell was not affected by partially photobleached Orai1-mGFP pores.

Tetrameric Assembly of Mobile Resting State Orai1—We applied the methodology for the characterized T24 cell line

overexpressing Orai1-mGFP. The TOCCSL method allowed for single molecule tracing (Fig. 3*D*); brightness estimates *B* were determined by integrating the signal above background within a 3 × 3 pixels region. Fig. 3*E* shows a typical time trace of the recorded single molecule brightness values. Data show significant fluctuations, precluding direct identification of accurate brightness levels arising from the stepwise photobleaching of the individual subunits. The main cause for the fluctuations was, besides on/off-blinking (34), the local background around the molecules, which varied significantly along the paths of the moving ion channels. We therefore reverted to a statistical analysis of the obtained brightness distributions. The described customized illumination protocols were applied to alternately image and partially photobleach the observed aggregates, so that individual trajectories consisted of a bright and a dim segment corresponding to higher and lower numbers of active mGFP label per spot.

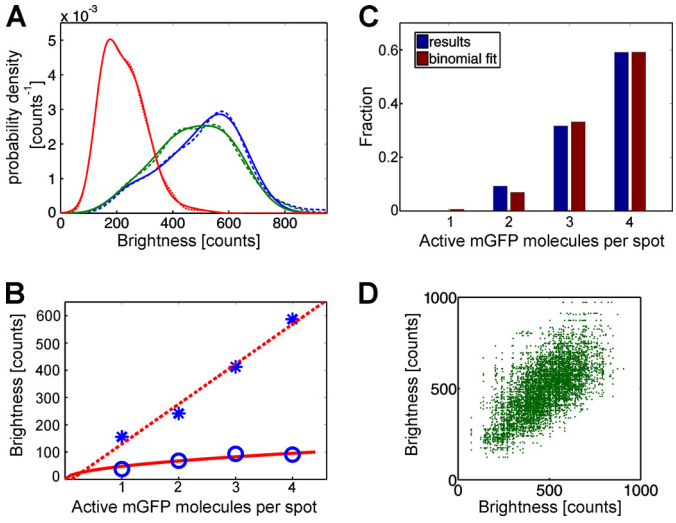

FIGURE 4. **Subunit stoichiometry of Orai1 pores.** *A*, brightness distributions of the three different data sets shown as *blue* (1), *green* (2), and *red* (3) *dotted curves*. Continuous lines show the fitted curves using the global fitting algorithm and a 4-Gaussian model. *B*, mean values (*asterisks*) and width (*circles*) of the individual Gaussians obtained using the tetramer model. The mean values show a linear increase, the widths increase with the square root (*red* fit curves). *C*, weights of the four individual Gaussians used to model data set 1 (*blue*). The distribution was well reproduced by a binomial distribution (*red*), yielding a probability of 0.88, which can be interpreted as the mGFP maturation degree. *D*, correlation plot of brightness values within individual trajectories. Each brightness value was plotted *versus* all preceding values of the same trajectory (data set 2), revealing strong correlation (Pearson's correlation coefficient of 0.65). All data were recorded at 37 °C.

The brightness values obtained in these segments were grouped into three distinct data sets (see Fig. 3*F* for assignment). Set 1 contains only data recorded in the first image after photobleaching and recovery (image *iii*); this set reveals the full label stoichiometry of the observed spots. Set 2 contains all brightness values recorded before the second bleaching pulse (the bright segment); in this case, photobleaching during the imaging sequence may influence the brightness levels. The corresponding distribution is therefore slightly shifted toward lower levels. Set 3 contains all data recorded after the second bleach pulse β (the dim segment), with a brightness distribution substantially reduced and shifted toward unitary GFP brightness.

The brightness distributions of the three data sets are shown in Fig. 4*A*. Each distribution shows distinct peaks and shoulders, indicating specific numbers of active GFP per observed spot. To jointly utilize the available information, we performed a global fit analysis of all three data sets. We reasoned that the mean and width of the individual peaks are the same over all sets, whereas the statistical weights may vary. The single fluorophore signals were approximated by Gaussian functions (26–28).

We first tested a model using four Gaussians, assuming a tetrameric state of Orai1 channels. The model fitted the data very well. We found equally spaced mean values of the oligomeric states *i*, with a single fluorophore brightness of ~156 counts (Fig. 4*B* and Table 1); apparently, the individual fluorophores emit independently, which was also observed in the stepwise photobleaching studies on GFP (18, 19) or in fluorescence fluctuation spectroscopy (35, 36). The width scales with the square root of *i* (Fig. 4*B*), as expected for a convolution of *i* Gaussian functions. We next analyzed the weights of the Gaussians α_{ij}, with *i* denoting the number of active mGFPs per pore, and *j* denoting the respective data set. Analysis of set 1 is shown in Fig. 4*C*; the weights α_{i1} were perfectly reproduced by a binomial distribution with four states and a probability of $p = 0.88$, which can be interpreted as the GFP matu-

TABLE 1

Comparison of fitting results using different models

Res_{norm} is the norm of the overall fitting residuals. The respective means μ_i, widths σ_i, and weights α_{ij} of the individual Gaussians obtained for each data set are included for comparison.

Model	Res_{norm} ($\times 10^6$)	μ_1/σ_1 (counts)	μ_2/σ_2 (counts)	μ_3/σ_3 (counts)	μ_4/σ_4 (counts)	μ_5/σ_5 (counts)	Data set	Weights of Gaussians describing different numbers of active mGFPs per Orai1 pore				
								1	2	3	4	5
2-Gaussian	26.10	212/78	515/141				1	0.05	0.95			
							2	0.08	0.92			
							3	0.98	0.02			
3-Gaussian	5.89	162/44	257/68	523/133			1	0.00	0.08	0.92		
							2	0.00	0.12	0.88		
							3	0.38	0.60	0.01		
4-Gaussian	1.12	156/38	241/69	412/96	587/92		1	0.00	0.09	0.32	0.59	
							2	0.00	0.08	0.47	0.45	
							3	0.27	0.70	0.04	−0.01	
5-Gaussian	0.40	157/40	248/63	389/62	499/142	597/63	1	0.00	0.07	0.01	0.72	0.20
							2	0.00	0.07	0.03	0.86	0.04
							3	0.33	0.63	0.03	0.01	0.00

ration degree. A similar degree of maturation was reported previously (18).

Recently, two models were reported regarding the oligomeric state of resting state Orai1, proposing a stable tetramer (16) or a dimer (17). We therefore tested whether a dimeric subunit stoichiometry could also give rise to our observed brightness distributions. In supplemental Fig. S3, we show a global fit to the three data sets, using a sum of two Gaussian functions. In this case, global fitting yields a single Gaussian peak describing data set 3; accordingly, sets 1 and 2 are best fitted by the second Gaussian peak at roughly twice the intensity (mean value of 220 *versus* 511 counts; see supplemental Fig. S3 and Table 1). If the dimer hypothesis was correct, set 3 would thus contain mainly the signal of single GFP molecules, and sets 1 and 2 would contain predominantly the signal of two colocalized GFP molecules. We argue below that this scenario is incorrect.

First, the fit curves deviate significantly from the data; the overall norm of the residuals is higher by a factor of 23 compared with the 4-Gaussian model (Table 1); by performing a nonparametric statistical test, we estimated a p value of 0.54 for the tetrameric model and only 0.02 for the dimeric model (see "Experimental Procedures" for a description of the test), indicating that the dimeric subunit assembly is less likely than a tetrameric. Second, we plotted each brightness value measured in an individual trajectory (x axis in Fig. 4*D*) *versus* all preceding brightness values obtained for the same trajectory (y axis). Correlation plots are shown for data set 2 representing the trajectory before the extra photobleaching pulse β. Interestingly, we found strong correlation (Pearson's correlation coefficient $c_{corr} = 0.65$), which is only consistent with the presence of extrinsic fluctuations, *i.e.* spots of inherently different brightness levels. In our case, the different brightness levels can be ascribed to the presence of spots containing different numbers of active mGFP molecules. Therefore, the strong correlation is in conflict with the dimer model, which would have required that nearly all spots originated from two active mGFP molecules. The validity of this argument was confirmed by Monte Carlo simulations (supplemental Fig. S4); the overall shape of the tetramer model agrees well with the data, yielding a similar correlation coefficient ($c_{corr} = 0.58$). Analogous simulations assuming a dimer model yielded two well separated symmetrical point clouds, characterized by a much broader spread and lower correlation coefficient $c_{corr} = 0.26$.

Trimeric and Pentameric Subunit Compositions Are Inconsistent with Observed Data—We also tested whether a trimeric or pentameric model could explain the observed data. First, we fitted the observed brightness distributions with a model assuming trimeric subunit composition. The fit was performed in an identical way as the tetrameric and dimeric model. Using the 3-Gaussian model, we found significant deviations from the data; the residuals were about five times larger compared with the 4-Gaussian model (Table 1 and supplemental Fig. S5).

Second, the 3-Gaussian model would only be consistent with the data, if data set 2 originated from a rather pure fraction of three active mGFP molecules per Orai1 spot; the fit yields $\alpha_{32} = 0.88$ (Table 1). Also, we performed Monte Carlo simulations for the expected brightness correlations of the 3-Gaussian model (supplemental Fig. S4*C*) yielding two well separated symmetrical point clouds. The simulated data differ significantly from the experimentally obtained results shown in Fig. 4*B*; in particular, a significantly reduced correlation coefficient of $c_{corr} = 0.31$ was estimated from the simulations.

Furthermore, we tested whether a pentamer of Orai1-mGFP subunits could account for the measured brightness distributions. For example, a pentameric assembly of Orai1 and Orai3 was found for arachidonate-regulated Ca^{2+}-channels (37). Zhou *et al.* (13) reported tetramers using disulfide cross-linking assays, but they did not exclude the possibility of higher oligomers.

Indeed, the pentameric model also fits the observed brightness distributions; the global fitting curves yielded residuals, which are by a factor ~3 smaller that of the tetrameric model (Table 1 and supplemental Fig. S6*A*). However, the fit parameters do not reflect a realistic scenario. First, the brightness distributions are not in accordance with the binomial model that typically describes the distribution of active GFP molecules on ion channels (supplemental Fig. S6*B*, *inset*) (16–18). Second, Gaussian number 4, which accounts for four active mGFP molecules per spot, yields an unrealistically large S.D., compared with the other Gaussians (Table 1).

In summary, only the 4-Gaussian model was able to reproduce the observed correlations.

DISCUSSION

We have presented a combined approach of photobleaching and single molecule brightness analysis to characterize the subunit composition of mobile plasma membrane proteins. The method is applicable for arbitrary expression levels, in particular when surface densities are too high for direct single molecule imaging. By restricting the readout to moving entities of similar mobility, an extremely pure fraction of molecules can be prepared for brightness and mobility analysis directly in the live cell plasma membrane. We implemented customized timing protocols for imaging and photobleaching to record distinctive data sets at different degree of active label and used global fitting to extract the subunit stoichiometry.

In this study, we employed our method to unravel for the first time the subunit composition of mobile resting state Orai1. We restricted our analysis to mobile Orai1 assemblies to rule out experimental biases, in particular to exclude potential coupling of the observed channels to STIM1 located in the ER. The results shed new light on the conflicting observations made by Ji *et al.* (16) and Penna *et al.* (17), who reported tetrameric Orai1 assemblies in fixed human cells and dimeric Orai assemblies in intact *Xenopus* oocytes, respectively. According to our single molecule and ensemble FRET data, in mammalian cells Orai1 forms stable tetramers, that do not need to further associate for activation. The Orai dimers observed by Penna *et al.* (17) in oocytes, however, may be taken as an indication that different regulatory mechanisms of the subunit stoichiometry could occur in different cell types.

REFERENCES

1. Parekh, A. B., and Putney, J. W., Jr. (2005) *Physiol. Rev.* **85,** 757–810
2. Hoth, M., and Penner, R. (1993) *J. Physiol.* **465,** 359–386
3. Zhang, S. L., Yu, Y., Roos, J., Kozak, J. A., Deerinck, T. J., Ellisman, M. H., Stauderman, K. A., and Cahalan, M. D. (2005) *Nature* **437,** 902–905
4. Liou, J., Kim, M. L., Heo, W. D., Jones, J. T., Myers, J. W., Ferrell, J. E., Jr., and Meyer, T. (2005) *Curr. Biol.* **15,** 1235–1241
5. Liou, J., Fivaz, M., Inoue, T., and Meyer, T. (2007) *Proc. Natl. Acad. Sci. U.S.A.* **104,** 9301–9306
6. Wu, M. M., Buchanan, J., Luik, R. M., and Lewis, R. S. (2006) *J. Cell Biol.* **174,** 803–813
7. Muik, M., Frischauf, I., Derler, I., Fahrner, M., Bergsmann, J., Eder, P., Schindl, R., Hesch, C., Polzinger, B., Fritsch, R., Kahr, H., Madl, J., Gruber, H., Groschner, K., and Romanin, C. (2008) *J. Biol. Chem.* **283,** 8014–8022
8. Park, C. Y., Hoover, P. J., Mullins, F. M., Bachhawat, P., Covington, E. D., Raunser, S., Walz, T., Garcia, K. C., Dolmetsch, R. E., and Lewis, R. S. (2009) *Cell* **136,** 876–890
9. Prakriya, M., Feske, S., Gwack, Y., Srikanth, S., Rao, A., and Hogan, P. G. (2006) *Nature* **443,** 230–233
10. Zhang, S. L., Yeromin, A. V., Zhang, X. H., Yu, Y., Safrina, O., Penna, A., Roos, J., Stauderman, K. A., and Cahalan, M. D. (2006) *Proc. Natl. Acad. Sci. U.S.A.* **103,** 9357–9362
11. Yeromin, A. V., Zhang, S. L., Jiang, W., Yu, Y., Safrina, O., and Cahalan, M. D. (2006) *Nature* **443,** 226–229
12. Gwack, Y., Srikanth, S., Feske, S., Cruz-Guilloty, F., Oh-hora, M., Neems, D. S., Hogan, P. G., and Rao, A. (2007) *J. Biol. Chem.* **282,** 16232–16243
13. Zhou, Y., Ramachandran, S., Oh-Hora, M., Rao, A., and Hogan, P. G. (2010) *Proc. Natl. Acad. Sci. U.S.A.* **107,** 4896–4901
14. Maruyama, Y., Ogura, T., Mio, K., Kato, K., Kaneko, T., Kiyonaka, S., Mori, Y., and Sato, C. (2009) *J. Biol. Chem.* **284,** 13676–13685
15. Mignen, O., Thompson, J. L., and Shuttleworth, T. J. (2008) *J. Physiol.* **586,** 419–425
16. Ji, W., Xu, P., Li, Z., Lu, J., Liu, L., Zhan, Y., Chen, Y., Hille, B., Xu, T., and Chen, L. (2008) *Proc. Natl. Acad. Sci. U.S.A.* **105,** 13668–13673
17. Penna, A., Demuro, A., Yeromin, A. V., Zhang, S. L., Safrina, O., Parker, I., and Cahalan, M. D. (2008) *Nature* **456,** 116–120
18. Ulbrich, M. H., and Isacoff, E. Y. (2007) *Nat. Methods* **4,** 319–321
19. Leake, M. C., Chandler, J. H., Wadhams, G. H., Bai, F., Berry, R. M., and Armitage, J. P. (2006) *Nature* **443,** 355–358
20. Zacharias, D. A., Violin, J. D., Newton, A. C., and Tsien, R. Y. (2002) *Science* **296,** 913–916
21. Schwarzenbacher, M., Kaltenbrunner, M., Brameshuber, M., Hesch, C., Paster, W., Weghuber, J., Heise, B., Sonnleitner, A., Stockinger, H., and Schütz, G. J. (2008) *Nat. Methods* **5,** 1053–1060
22. Xia, Z., and Liu, Y. (2001) *Biophys. J.* **81,** 2395–2402
23. Hesse, J., Sonnleitner, M., Sonnleitner, A., Freudenthaler, G., Jacak, J., Höglinger, O., Schindler, H., and Schütz, G. J. (2004) *Anal. Chem.* **76,** 5960–5964
24. Wieser, S., and Schütz, G. J. (2008) *Methods* **46,** 131–140
25. Goulian, M., and Simon, S. M. (2000) *Biophys. J.* **79,** 2188–2198
26. Schmidt, T., Schutz, G. J., Gruber, H. J., and Schindler, H. (1996) *Anal. Chem.* **68,** 4397–4401
27. Mashanov, G. I., Nobles, M., Harmer, S. C., Molloy, J. E., and Tinker, A. (2010) *J. Biol. Chem.* **285,** 3664–3675
28. van Zanten, T. S., Cambi, A., Koopman, M., Joosten, B., Figdor, C. G., and Garcia-Parajo, M. F. (2009) *Proc. Natl. Acad. Sci. U.S.A.* **106,** 18557–18562
29. Wieser, S., Axmann, M., and Schütz, G. J. (2008) *Biophys. J.* **95,** 5988–6001
30. Axelrod, D. (2001) *Traffic* **2,** 764–774
31. Woodard, G. E., Salido, G. M., and Rosado, J. A. (2008) *Am. J. Physiol. Cell Physiol.* **294,** C1323–1331
32. Moertelmaier, M., Brameshuber, M., Linimeier, M., Schutz, G. J., and Stockinger, H. (2005) *Appl. Phys. Lett.* **87,** 263903
33. Ruprecht, V., Brameshuber, M., and Schutz, G. J. (2010) *Soft Matter* **6,** 568–581
34. Garcia-Parajo, M. F., Segers-Nolten, G. M., Veerman, J. A., Greve, J., and van Hulst, N. F. (2000) *Proc. Natl. Acad. Sci. U.S.A.* **97,** 7237–7242
35. Müller, J. D., Chen, Y., and Gratton, E. (2000) *Biophys. J.* **78,** 474–486
36. Chen, Y., Wei, L. N., and Müller, J. D. (2003) *Proc. Natl. Acad. Sci. U.S.A.* **100,** 15492–15497
37. Mignen, O., Thompson, J. L., and Shuttleworth, T. J. (2009) *J. Physiol.* **587,** 4181–4197